Geochemistry, Geophysics, Geosystems®

AGU ADVANCING EARTH AND SPACE SCIENCES

RESEARCH ARTICLE
10.1029/2023GC011202

Key Points:

- We present a user-friendly approach for determining trace element to calcium ratios using readily accessible and easy to use instrumentation
- This method requires an extremely small sample size, <40 μg of $CaCO_3$, for determining trace elemental ratios with an excellent limit of detection
- Our method is characterized by better than 1% accuracy and precision during determination of TE/Ca using both ICP-OES and ICP-QQQ-MS

Supporting Information:

Supporting Information may be found in the online version of this article.

Correspondence to:

I. V. Satya Chanakya,
satya.ivs6@gmail.com

Citation:

Satya Chanakya, I. V., & Misra, S. (2024). Determination of trace elemental composition of $CaCO_3$: Application to mass limited abiogenic and biogenic carbonates. *Geochemistry, Geophysics, Geosystems*, *25*, e2023GC011202. https://doi.org/10.1029/2023GC011202

Received 6 SEP 2023
Accepted 5 JAN 2024

Author Contributions:

Conceptualization: I. V. Satya Chanakya, Sambuddha Misra
Formal analysis: I. V. Satya Chanakya
Funding acquisition: Sambuddha Misra
Investigation: I. V. Satya Chanakya
Methodology: I. V. Satya Chanakya
Project administration: Sambuddha Misra
Resources: Sambuddha Misra
Software: I. V. Satya Chanakya
Supervision: Sambuddha Misra
Visualization: I. V. Satya Chanakya
Writing – original draft: I. V. Satya Chanakya, Sambuddha Misra

Determination of Trace Elemental Composition of $CaCO_3$: Application to Mass Limited Abiogenic and Biogenic Carbonates

I. V. Satya Chanakya[1] and **Sambuddha Misra**[1]

[1]Centre for Earth Sciences, Indian Institute of Science, Bangalore, India

Abstract An improved method for accurate and precise determination of metal to calcium ratio in mass limited calcium carbonate samples has been developed. We used an Agilent®5800 ICP-OES for major element (Na/Mg/Sr to Ca) and an Agilent®8900 ICP-QQQ-MS for minor and trace element (Li/B/Na/Mg/Al/Mn/Fe/Zn/Sr/Cd/Ba/U to Ca) ratio determination. We report a long-term precision of ≤1% (1σ) by repeat analysis, spread over ≥6 analytical sessions, of multiple external standards that spanned a large range of concentration. We quasi-quantitatively eliminated potential matrix effect from high [Ca] by concentration matching samples and standards (Δ[Ca] ≤ ±5%) during both ICP-OES and ICP-QQQ-MS sessions. The ICP-OES analyses were done on 200 μl of sample at 60 ppm [Ca], consuming ~30 μg of $CaCO_3$ per analysis. Whereas trace element analyses by ICP-QQQ-MS required ~150 μl of sample at 20 ppm [Ca], consuming ~7.5 μg of $CaCO_3$ per analysis. Thus, the present method allows for high precision determination of TE/Ca in <40 μg of $CaCO_3$. We present a comprehensive approach for optimization of ICP-OES sensitivity and stability to select elemental (Ca/Na/Mg/Sr) wavelengths with minimal interferences, high sensitivity and linearity. For choice of Ca lines, we focused on the minimization of self-matrix effect. For the ICP-MS method, we improved reproducibility and precision by lowering [Ca] of analyte and preconditioning of cones. Furthermore, the present method allows for precise B/Ca determination sans the use of HF matrix. In summary, we present an easily adoptable method based on readily available instrumentation for determining element-to-calcium ratios that is suitable for analyzing mass-limited carbonate samples.

1. Introduction

The concentration and isotopic composition of the trace level impurities hosted within the carbonate lattice of biogenic and abiogenic calcium carbonates are widely utilized in the fields of paleoceanography and geochemistry (Boyle, 1988; Elderfield & Ganssen, 2000; Hall & Chan, 2004; Marchitto et al., 2000). Elemental ratios (ME/Ca) like Li/Ca, B/Ca, Na/Ca, Mg/Ca, Sr/Ca, Mn/Ca, Cd/Ca, Ba/Ca, and U/Ca of biogenic carbonates have widespread application in quantitative reconstruction of past climatic conditions. Each of these ME/Ca in biogenic carbonates vary as a function of one or more physiochemical parameters of seawater with possible secondary influence via carbonate precipitation pathway (Bentov & Erez, 2006; Toyofuku et al., 2000).

The commonly utilized paleoceanographic proxies are: (i) Li/Ca and B/Ca of benthic foraminifera for deep water (in situ) carbonate ion saturation state and concentration respectively (Allen et al., 2012; Lear et al., 2002; Marriott et al., 2004; Yu et al., 2007), Ba/Ca also used as a productivity and pollution tracer in marine carbonates (Foster et al., 2008), Na/Ca of planktonic foraminifera for salinity (Wit et al., 2013), Mg/Ca of both planktonic and benthic foraminifera for reconstruction of calcification temperature (Delaney et al., 1985; Lea et al., 1999; Rosenthal et al., 1997), Mn/Ca for nutrient concentrations of surface water (Marr et al., 2013), Sr/Ca for calcification rate and the state of preservation of sedimentary calcite (Barker et al., 2003; Elderfield et al., 2002; Kısakürek et al., 2008; Lea et al., 1999; Stoll et al., 1999), and secular changes in seawater $[Sr]_{SW}$ over geologic time (Billups et al., 2004; Martin et al., 2000; Stoll et al., 1999), Sr/Ca is widely used in scleractinian corals as a sea surface temperature (Steinhardt et al., 2016), Mn/Ca and Sr/Ca is also used as temperature or pollution indicators in freshwater bivalves (Carroll et al., 2009), Ba/Ca for quantification of freshwater run off (nutrient supply) (Hall & Chan, 2004), Cd/Ca for in situ phosphate concentration (ross rickaby) (Boyle, 1988; Delaney, 1989; Yu et al., 2013), and U/Ca for quantification of $[CO_3^{2-}]$ and pH (Russell et al., 2004). These proxies commonly demonstrate a species-specific sensitivity to the controlling parameter(s) (Allen et al., 2016).

Writing – review & editing: I. V. Satya Chanakya, Sambuddha Misra

The primary and secondary controllers of elemental ratios and their sensitivity are quantified by laboratory calibration of a few specimens of extant species (Bentov & Erez, 2006; Nehrke et al., 2013; Smith et al., 2020). A species-specific approach needs to be adopted for planktonic foraminifera due to differences in their depth habitat and the sensitivity of proxies to external forces; this restricts the sample size. Additionally, intervals of the earth's history which demonstrate high amplitude and frequency of climate change are usually characterized by decreased availability of biogenic carbonates and poor preservation state (Broecker & Clark, 2004). Thus, it is critical to have a robust method for the determination of ME/Ca from mass limited samples.

Marine biogenic carbonates, especially calcite, contains nominal amount of metallic impurity (~99% pure $CaCO_3$). The concentration of these impurities in pure biogenic calcite ranges from mmol/mol (Mg, Sr) to nmol/mol (Cd, U) (Boyle, 1988). Since the majority of these trace elements are in extremely low abundance, a significant mass of carbonate is required to achieve analyte concentrations above the instrumental detection limit. This results in a relatively high concentration of Ca in the dissolved fraction. Analysis of this high Ca solution can lead to precipitation of Ca on the ICP-MS interface resulting in large and variable instrumental drift along with considerable loss in sensitivity of other analytes (Yu et al., 2005).

There exists a large difference in the absolute abundance of trace metal (approximately an order of magnitude) between different foraminiferal species and within specimens of the same species of different sizes (Allen et al., 2016; Bentov & Erez, 2006; Lea et al., 1999). Thus, the palaeoceanographic community must adopt a size-fraction specific and species-specific approach for achieving high precision paleo-climatic reconstruction, thereby limiting the mass of material available per sample/age interval. This mass limitation is ubiquitous and is a constraining factor for both biogenic and abiogenic samples. For example, during precipitation experiments small masses of $CaCO_3$ (~mg) are harvested to ensure precipitation under quasi-constant solution composition, whereas for coral based reconstruction a nominal amount of material is available from individual growth bands.

Natural biogenic carbonate requires chemical cleaning to remove clays, organic matter, and post-depositional overgrowth of secondary mineral phases (Fe-Mn oxy-hydroxides) (Lea & Martin, 1996; Lear et al., 2002). The multi-step chemical cleaning results in a variable amount of mass loss during each step culminating in a significant (20%–60%) total mass loss. Thus, most measurements become restricted to a fractions of mg (0.2–0.5 mg) of $CaCO_3$ samples, resulting in micrograms to picograms of analyte. Furthermore, during ICP-MS determination the presence of plasma based polyatomic isobaric interferences such as $^{40}Ar^{16}O$ on ^{56}Fe, and $^{40}Ar^{15}$ N on ^{55}Mn undermines the accuracy of the analysis. In addition, marine carbonates are characterized by extremely low concentrations of elements belonging to either end of the periodic table and transition metals. For example, Li/Ca, and U/Ca ratios typically ranges between 1–5 and 5–7 nmol/mol respectively. So, the ideal analytical strategy must involve a mass spectrometer which has comparable sensitivity across the periodic table.

To overcome these analytical challenges and to consistently maintain high accuracy and precision, we require instrument(s) characterized by: (a) high sensitivity across the mass range; (b) consistent sensitivity across a large range of concentration for all masses (linear calibration curve); and (c) minimal drift in sensitivity over time (high stability) even at significant total dissolved solid (TDS) load. The ICP-OES and ICP-MS, inductively coupled plasma-based instruments, provide an opportunity for swift and precise determination of elemental ratios (ME/Ca) across the periodic table at high TDS load. In this study we focus on the application of ICP-OES and ICP-QQQ-MS due to their ease of operation and widespread availability. The ICP-OES was utilized to determine the metal to calcium ratio of major and minor elements such as Na, Mg, and Sr. The simultaneous and accurate determination of the metals, at their respective emission wavelengths, by ICP-OES allows for high precision ($\leq$1%, 2σ) determination of these ratios. For metals with concentrations above 100 ng/ml in the samples matrix (at [Ca] between 20 and 100 ppm), it is preferable to measure them by ICP-OES provided there are no major spectral interferences from argon or calcium on these elements, Whereas the concentration of metals (viz. Li, B, Mn, Fe, Cd, Ba, and U) with low abundance in carbonate samples was determined by ICP-QQQ-MS. This instrument allows for precise and accurate determination of ME/Ca ratio due to (a) fast scan time (0.1 ms) across the mass range (Li to U); (b) improvement in sensitivity (~300%) relative to prior models of QICP-MS; (c) comparable sensitivity across the entire mass range; (d) quasi constant sensitivity over a concentration range spanning 6–7 orders of magnitude; and (d) instrumental ability to resolve isobaric polyatomic interferences from analyte masses utilizing chemical (collision reaction cell (CRC)) resolution.

During quantification of ME/Ca, metals are commonly categorized into major, minor and trace depending on their concentration in carbonate samples (Allen et al., 2016; Lea & Martin, 1996). Major elements make up more than

0.4% of a substance by weight, while minor elements make up between 0.1% and 0.4%, and trace elements make up less than 0.1%. Traditionally the major and minor elements are measured by ICP-OES whereas the trace elements are determined by high sensitivity sector field ICP-MS mass spectrometers (Marchitto et al., 2000; Misra et al., 2014; Rosenthal et al., 1997) or quadrupole ICP-MS (Yu et al., 2005). ICP-MS based determination methods utilize a combination of matrix matching external calibration, internal standard addition, and/or isotope dilution for accurate determination of trace elemental ratios and concentrations (Lea & Martin, 1996).

Sector field mass spectrometers, characterized by high sensitivity, allows for precise determinations of low abundance elements like Li, Cd, and U. Among the commonly adopted strategy for analysis, isotope dilution involves spike calibration of sophisticated instrumentation followed by complex calculations. Successful application of isotope dilution requires measuring a minimum of two isotopes per element which increases analysis time, resulting in relatively larger mass consumption. Additionally, different isotopes of the same element might have interferences originating from different sources (plasma vs. matrix) thus, requiring a complex analysis strategy (Boyle, 1981) (E. A. Boyle & Keigwin, 1985; Marchitto et al., 2000). For analysis of elements with potential polyatomic interference(s), multiple resolution modes (Fe, Mn in medium resolution, and K in high resolution) are used. In addition, calcium has to be measured in each resolution mode for accurate metal to calcium ratio determination. As a result, there is a considerable increase in analysis time per sample. We present an accelerated measurement approach using ICP-QQQ-MS that offers comparable or superior accuracy and precision across the spectrum (from Li to U) while minimizing sample mass requirements.

We outline a three-step method for the determination of metal to calcium ratio in biogenic and abiogenic carbonates. In the first step, the calcium concentration of the sample is determined by ICP-OES against external calibration standards of varying calcium concentration. In the second step, the minor element (Na, Mg, and Sr) to calcium ratios are determined by ICP-OES against a series of external calibration standards (containing variable amounts of metals) at a fixed calcium concentration of 60 ppm. In the final step, the trace metal (Li, B, Na, Mg, Fe, Mn, Sr, Cd, Ba, and U) to calcium ratios were determined against an external multi-element calibration at a fixed calcium concentration of 20 ppm on ICP-QQQ-MS. For both ICP-OES and ICP-MS determinations, the samples are analyzed at close calcium concentration matching ($\leq \pm 5\%$) with standards. Elements like Li, B, Na, Mg, Al, Sr, Cd, Ba, and U which does not have any significant polyatomic isobaric interferences were measured in non-CRC mode. Elements like K, Mn, and Fe, which have significant argon-based polyatomic isobaric interferences, were measured in the CRC mode (H_2 + He). For mass-limited samples, the CRC mode was exclusively utilized for the determination of all elements irrespective of potential isobaric interference(s) with identical accuracy. This strategy significantly reduces the ICP-MS analysis time per sample, which allows for the analysis of samples with <10 μg of $CaCO_3$.

Only a few studies have extensively explored the optimization strategy for minor element to calcium ratio determination (Na/Ca, Mg/Ca, Sr/Ca) via ICP-OES. The impact of parameters like selection of wavelength based on the choice of detection mode (axial vs. radial) or the importance of plasma/torch parameters (de Villiers et al., 2002) during determination of ME/Ca ratio in calcium-rich matrices by ICP-OES remains poorly explored. Similarly, there is a limited number of studies (Yu et al., 2005) that offer a comprehensive strategy for optimizing the determination of trace metal to calcium ratios from calcium-rich matrices using Q-ICP-MS. Factors such as the selection of isotope for concentration measurement, mode of detection, and optimization of calcium concentration for best results, and tolerance for calcium concentration mismatch have not been exhaustively explored. In summary, we provide an easy to adopt strategy for accurate and precise determination of metal to calcium ratio (from Li/Ca to U/Ca) in carbonates. This improved method requires a small sample size of ∼22.5 μg of $CaCO_3$ per analysis including ICP-OES and ICP-QQQ-MS with precision of ∼1% across the mass range. Most importantly, this method presents a non-HF approach to determining the B/Ca ratio.

2. Materials and Methods

2.1. ICP-OES

The concentration of the major and minor elements was determined by an Agilent 5800 ICP-OES installed at the Indian Institute of Science (IISc), Bangalore. An optimized method for the determination of carbonate hosted major and minor elements by ICP-OES was developed. The present method requires a small sample volume of 100–150 μl per analyses at a calcium concentration of 60 ppm. The method was optimized for a sample analysis time of ∼85 s, which includes 55 s of uptake time, 10 s of stabilization time, and 18 s of analysis time (for both

Table 1
ICP-OES Settings for Minor ME/Ca Determinations

ICP-OES parameters	Optimal setting (axial/radial)
Operating conditions of ICP-OES	
Nebulizer	Concentric self-aspirating
Uptake rate	80 µl/min
Spray chamber	quartz cyclonic
RF Power (kW)	1.2/1.4
Plasma gas flow (L/min)	14/13
Auxiliary gas flow (L/min)	0.7/1.0
Nebulizer flow (L/min)	0.8/0.4
Wash time (s)	120 s
Uptake time	55 s
Stabilization time	10 s
Read time (s)	3
Replicates	3
Plasma viewing position	Axial, radial

radial and axial modes of detection). Thus, the present method is optimized for precise determination of minor elements to calcium ratio (Na/Ca, Mg/Ca, and Sr/Ca) utilizing 15–22.5 µg of $CaCO_3$.

The Agilent 5800 has an axially viewed plasma which offers concurrent dual viewing modes, with possible detection of ions in either radial mode (in a direction perpendicular to the plasma) or/and in the axial mode (in a direction parallel to the plasma). This instrument allows for simultaneous determination of metals and metalloids across a wavelength range of 167–785 nm. The instrument is equipped with a Charge Coupled Device detector with anti-blooming protection on each pixel and is maintained at a constant temperature of −40°C. This ensures that there is minimal to zero back scattering of electrons to neighboring pixels even when a certain pixel is saturated with a large ion beam. Thus, accurate determination of neighboring wavelengths with orders of magnitude difference in intensity is possible. As a result, this improved technology allows us to measure the metal concentrations below 50–100 ppb in the presence of one or more dominant matrix elements. The intensity of emission at a particular wavelength is a function of the concentration of the element(s) with matching emission wavelength, the efficiency of nebulization and ionization and rate of sample introduction. The typical operating conditions for ICP-OES is given in Table 1.

A combination of a PFA concentric nebulizer with an aspiration rate of ∼80 µl/min and a quartz spray chamber of cyclonic design were utilized for sample introduction. Instrumental settings for best sensitivity and stability, in both radial and axial modes, were determined by optimizing for plasma gas, auxiliary gas, viewing height and nebulizer gas flows. For the optimization experiments, we focused on carbonate hosted major (Ca) and a selection of important minor (Na, Mg, and Sr) elements. The final selection of wavelength(s) for each element was based on their respective sensitivity, stability, linearity across the desired concentration range, and the presence or absence of any plasma or matrix-based optical interference(s). The optimization procedure is discussed in detail in the results and discussion section. Following the ICP-OES determination of major and minor elements, the same samples were analyzed for trace elemental ratios such as Li/Ca, B/Ca, Al/Ca, U/Ca etc. on the ICP-QQQ-MS.

Table 2
ICP-QQQ-MS Setting for Minor and Trace ME/Ca Determinations

ICP-QQQ-MS parameters	Optimal setting
Nebulizer	Concentric self-aspirating
Uptake rate	60 µl/min
Spray chamber	Quartz scott type
RF power (W)	1,500
Sample depth	4.5 mm
S/C temperature	2°C
Sampler cone	Platinum
Skimmer cone	Platinum
Sample matrix	0.1 M HNO_3
Uptake time	55 s
Stabilization time	10 s
Washout time	180 s
Acquisition time	∼30 s
Replicates/sweeps	9/9

2.2. ICP-QQQ-MS

The trace element to calcium ratios were determined by a quadrupole ICP-MS (Agilent 8900), equipped with CRC, installed at the IISc, Bangalore. Depending on the presence or absence of plasma/matrix based isobaric interferences, the elements were determined in either normal mode (Li, B, Na, Mg, Al, Zn, Sr, Ba, Cd, U) or in collision reaction mode (K, Fe, Mn). Calcium was determined in both modes for better accuracy and precision of each ME/Ca ratio. The optimal operating condition of the instrument is outlined in Table 2. In short, a combination of a PFA concentric nebulizer with an uptake rate of ∼60 µl/min and a Peltier cooled Scott-type quartz spray chamber was used for sample introduction. Prior to each analytical session, the instrument was optimized for sensitivity, stability, removal of interferences in CRC, and levels of oxide and doubly charged formation by tuning for torch position, nebulizer and dilution gas flows, lens parameters, and CRC gas flow rates and operational parameters. Optimization was done for the entire mass range from Li to U. We investigated the impact of integration time of a particular isotope on the accuracy and precision during ICP-QQQ-MS based measurements. Isotope specific integration time is provided in Table 3. This method enables the utilization of ICP-OES solely for the measurement of minor elements such as Na, Mg, and Sr. Furthermore, this approach can be expanded to analyze both minor elements (Na, Mg, and Sr) and trace elements (Li, B, Al, K, Mn, Fe, Zn, Ba, Cd, U) exclusively through ICP-QQQ-MS.

Table 3
The Duration of Integration Time Used in the Analysis Conducted on ICP-QQQ-MS

Element/Isotope	Integration time (s)
^{7}Li	0.1
^{11}B	0.1
^{23}Na	0.1
^{25}Mg	0.1
^{27}Al	0.1
^{43}Ca	0.1
^{55}Mn	0.2
^{56}Fe	0.2
^{66}Zn	0.1
^{87}Sr	0.1
^{113}Cd	0.2
^{137}Ba	0.1
^{238}U	0.2

Table 4
Limit of Detection for Various ME/Ca on ICP-QQQ-MS

ME/Ca	Mode	LOD	Units
^{7}Li/^{43}Ca	No gas	0.258	μmol/mol
^{11}B/^{43}Ca	No gas	1.356	μmol/mol
^{23}Na/^{43}Ca	Gas	0.037	mmol/mol
^{24}Mg/^{43}Ca	Gas	0.019	mmol/mol
^{25}Mg/^{43}Ca	No gas	0.022	mmol/mol
^{25}Mg/^{43}Ca	Gas	0.008	mmol/mol
^{27}Al/^{43}Ca	No gas	0.001	mmol/mol
^{27}Al/^{43}Ca	Gas	0.001	mmol/mol
^{55}Mn/^{43}Ca	Gas	1.663	μmol/mol
^{56}Fe/^{43}Ca	Gas	0.001	μmol/mol
^{66}Zn/^{43}Ca	No gas	0.278	μmol/mol
^{66}Zn/^{43}Ca	Gas	0.240	μmol/mol
^{87}Sr/^{43}Ca	No gas	0.024	μmol/mol
^{87}Sr/^{43}Ca	Gas	0.017	μmol/mol
^{87}Sr/^{43}Ca	No gas	0.018	μmol/mol
^{87}Sr/^{43}Ca	Gas	0.021	μmol/mol
^{111}Cd/^{43}Ca	No gas	0.012	μmol/mol
^{113}Cd/^{43}Ca	No gas	0.024	μmol/mol
^{114}Cd/^{43}Ca	No gas	0.009	μmol/mol
^{137}Ba/^{43}Ca	No gas	0.106	μmol/mol
^{137}Ba/^{43}Ca	Gas	0.167	μmol/mol
^{138}Ba/^{43}Ca	No gas	0.123	μmol/mol
^{138}Ba/^{43}Ca	Gas	0.095	μmol/mol
^{238}U/^{43}Ca	No gas	0.398	nmol/mol
^{238}U/^{43}Ca	Gas	0.895	nmol/mol

The CRC was optimized by monitoring the signal to noise ratio on ^{39}K, ^{55}Mn, ^{56}Fe, and ^{80}Se which are characterized by significant argon-based polyatomic interferences (^{38}Ar^{1}H on ^{39}K, ^{39}Ar^{14}N on ^{55}Mn, ^{40}Ar^{16}O on ^{56}Fe and ^{40}Ar^{40}Ar on ^{80}Se). The strategy for CRC tuning focused on optimization of H_2 and He gas flows (mixed gas mode) and cell parameters to achieve best signal to noise ratio on these specific masses. During a typical analytical session, the sensitivities for ^{7}Li, ^{43}Ca, and ^{238}U in normal analysis mode were approximately 700,000, 10,000, and 200,000 cps/ppb, respectively. Under optimal CRC operational conditions, we achieved ^{80}Se counts of 100–500 per s in 2% HNO_3 (v/v). In CRC mode the sensitivities for ^{39}K, ^{55}Mn, and ^{56}Fe were 143,000, 377,000, and 422,000 cps/ppb respectively. Under optimized instrumental operational conditions, the typical signal-to-noise ratios for ^{7}Li, ^{56}Fe, and ^{55}Mn were 2,600, 47, and 190 respectively. The signal to noise ratio for all the elements is given in Table 4.

2.3. Sample Preparation and Analysis

Five to ten specimens of foraminifera of the same species from 300 to 355 μm size fraction were handpicked under an optical microscope. The foraminifera specimens were carefully cracked open using a scalpel and then chemically cleaned, leached with weak acid, and dissolved in 0.5 M HNO_3.

The chemical cleaning process involves: (a) the removal of clay particles by repeated sonication with MQ and methanol, (b) the removal of organic matter by oxidative cleaning with 1% H_2O_2 in 0.1 N NaOH, and (c) for select samples, the removal of iron and manganese oxy-hydroxide phases through reductive cleaning (hydrazine and ammonium hydroxide/Ammonium hydroxide and citric acid buffer). Post chemical cleaning, the samples were transferred to a new, pre-cleaned vial for weak acid leach. Samples designated for boron isotope analysis underwent an additional leaching step with 1% double distilled ammonia, prior to weak acid leach with 0.001 N HNO_3. After the leaching, the samples were dissolved in 200–250 μl of 0.5 N double distilled nitric acid (depending on the total mass of the sample). The dissolved samples were then centrifuged, and the supernatant was transferred to a fresh, acid-cleaned vial, leaving behind a ∼10 μl residue.

The samples were first analyzed for Ca concentration by ICP-OES at a 1:10 dilution (total analyte volume ∼200 μl). Following which Na/Ca, Mg/Ca, and Sr/Ca (minor elements) were determined by the ICP-OES at a fixed Ca concentration of 60 ppm against multi-element external calibration. Standards and samples were analyzed at identical concentration (within 5% Ca concentration matching). Following which the samples were analyzed on quadrupole ICP-MS for TE/Ca (trace elements) at a fixed Ca concentration of 20 ppm. During Q-ICP-MS runs, a similar strategy of external calibration utilizing multi-element standards were adopted.

3. Development of the Instrument Method

The optimization of ICP-OES and ICP-QQQ-MS are discussed individually. The ICP-OES section is divided into two parts for ease of understanding.

3.1. Sample Preparation and Analysis

The instrument was optimized for maximum sensitivity by tuning for gas flows, viewing height of the plasma (in the radial mode) and plasma power. The selection of acquisition wavelength for each element was determined based on their sensitivity, the presence or absence of spectral interferences,

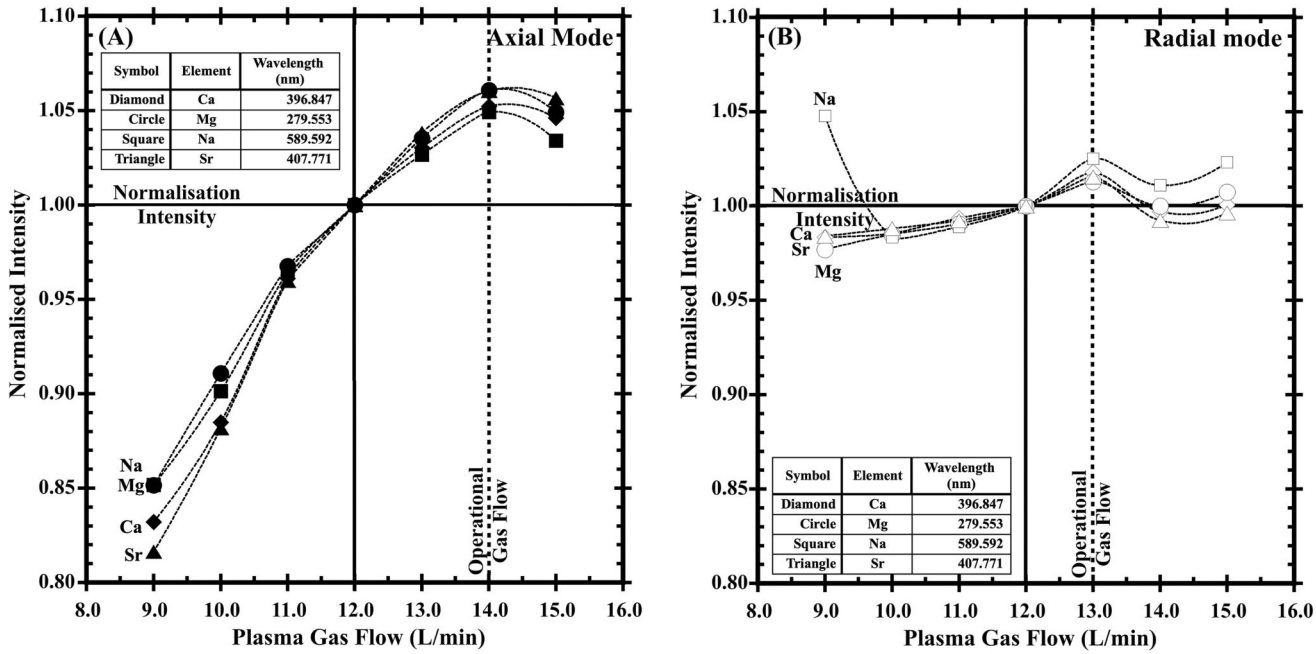

Figure 1. Variation in signal intensity for Ca, Mg, Na, and Sr for different plasma gas flow rates (in L/min) under typical operation conditions. The plasma gas flow rate is plotted on *x*-axis with normalized intensity (counts per second) on the *y*-axis. Panel (a) axial mode of acquisition; Panel (b) radial mode of acquisition. The normalized intensities are denoted by the following symbols: Ca-diamond, Mg-circle, Na-square, and Sr-triangle. The solid and open symbols represent the analysis performed in axial and radial mode respectively. The axial mode exhibits a greater change in intensity for a given change in gas flow.

and the linearity of sensitivity across a large analyte concentration range (10 s of ppb to 100 s of ppm). The magnitude of change in sensitivity resulting from changes in gas flow rate was significantly more in the axial mode than in the radial mode. Whereas in the radial mode of detection (detector positioned perpendicular to the torch), the sensitivity is strongly dependent on the viewing height. However, in the axial mode of detection (detector positioned parallel to the torch) the viewing height has minimal to no impact on sensitivity. Since this sensitivity optimization strategy involves tuning for gases and viewing height, it ensures minimal instrument drift over long analytical sessions (6–8 hr).

Optimization of ICP-OES operational conditions, which includes selection of gas flows for select elements, is discussed in the following sections.

3.1.1. Plasma Gas Flow

The impact of plasma gas flow rate on elemental sensitivity was investigated through a series of controlled experiments where the plasma gas flow rate was varied between 9.0 to 15.0 L/min (Figure 1) while keeping all other parameters constant. Irrespective of the choice of observational line, the element specific sensitivities demonstrate a uniform trend with plasma gas flow rate. Maximum intensity of the elemental line was observed at a plasma gas flow rate of 14 L/min in the axial mode and at 13 L/min in the radial mode. In radial mode, a minimal drop in sensitivity (1%–2%) was observed for ±1.0 L/min change in gas flow rate from optimal settings. Whereas in axial mode this drop in sensitivity was more significant, ∼5% during a decrease in gas flow and ∼2% during an increase in gas flow. The contrasting response of sensitivities to plasma gas flow was observed for alkali and alkali earth elements (Figure 1). The operational gas flows for ICP-OES were selected based on Na, Mg, Ca, and Sr. We observed a more significant change in sensitivity (∼5 fold) in axial mode over radial mode for a given change in gas flow.

3.1.2. Optimization of Auxiliary Gas Flow Rate

The impact of auxiliary gas flow on sensitivity was investigated by varying the auxiliary flow rate between 0.7 to 1.3 L/min while holding all other parameters constant including other gas flow rates (Figure 2). The maximum sensitivity is observed at the auxiliary gas flow rate of 0.7 and 1.0 L/min for axial and radial mode respectively.

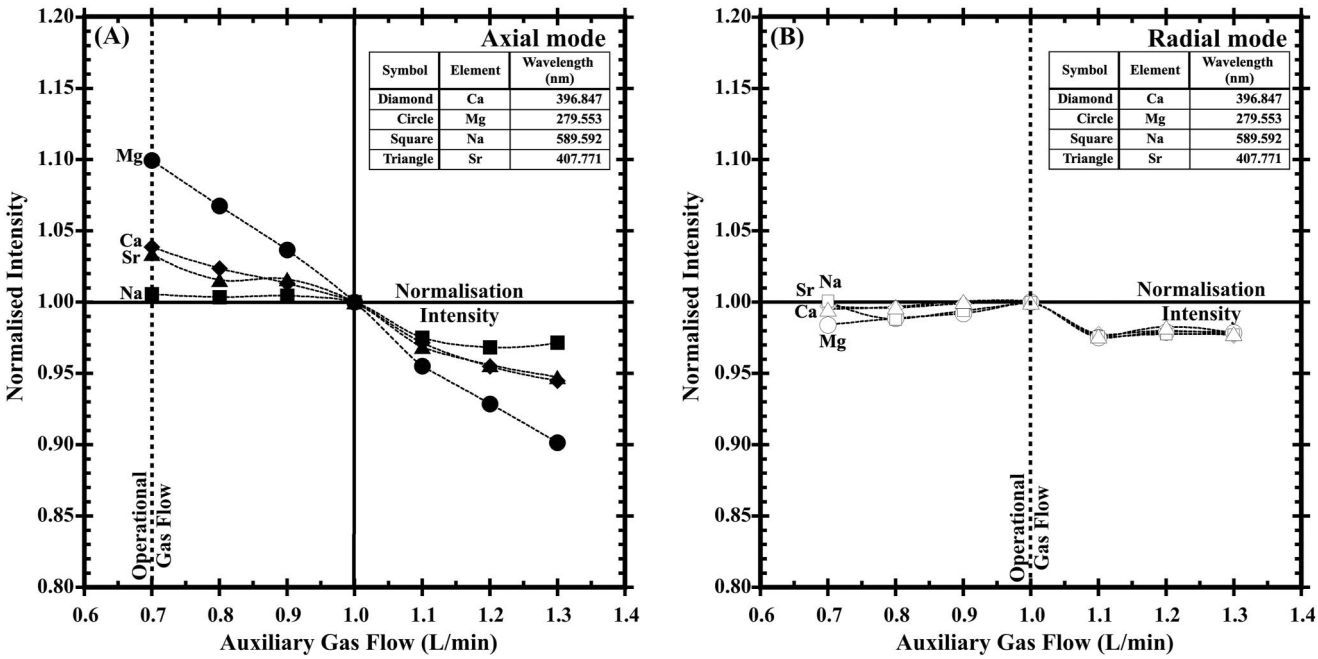

Figure 2. Variation in signal intensity for Ca, Mg, Na, and Sr for different auxiliary gas flow rates (in L/min) under typical operation conditions. The auxiliary gas flow rate is plotted on *x*-axis with normalized intensity (counts per second) on the *y*-axis. Panel (a) axial mode of acquisition; Panel (b) radial mode of acquisition. The normalized intensities are denoted by the following symbols: Ca-diamond, Mg-circle, Na-square, and Sr-triangle. The solid and open symbols represent the analysis performed in axial and radial mode respectively. The axial mode exhibits a greater change in intensity for a unit change (0.1 L/min) in gas flow.

For a unit change (0.1 L/min) in gas flow rate a 2%–4% drop in sensitivity was observed in radial mode whereas in the axial mode it was about 5%.

3.1.3. Optimization of Nebulizer Gas Flow Rate

The impact of nebulizer gas flow on sensitivity was investigated by varying the nebulizer flow rate between 0.4 to 1.0 L/min while holding all other parameters constant including other gas flow rates. The maximum sensitivity in radial mode is observed at gas flow rate of 0.4 L/min whereas in axial mode different metals exhibit maximum sensitivity at different flow rates (Figure 3). A flow rate of 0.8 L/min was selected in axial mode to maintain optimal sensitivity for all metals of interest. Note, that a flow rate of 0.6 L/min will result in maximize precision on Mg/Ca. The sensitivity in axial mode is more responsive to the change in gas flow rate, thus it is critical to optimize gas flow rate for best precision.

3.1.4. Determination of Viewing Height

The plasma viewing height of the ICP-OES is defined as (a) the distance of the tip of the torch from the detector in axial mode, and (b) in radial mode, it is defined as the angle of torch to the detector. The sensitivity in the radial mode is strongly dependent on the viewing height whereas in the axial mode it has minimal to no impact on sensitivity (Figure 4). Different elements, based on their ionization potential, ionize at different zones of the plasma. Thus, for optimal ionization in radial mode, it is critical to select a viewing height that ensures maximum ionization of elements of interest.

3.1.5. Plasma Power

Changes in the plasma power dominantly controls the signal intensity irrespective of the choice of other instrumental settings/tuning parameters. The choice of forward R.F. power determines the ionization efficiency and the zone of optimal ionization within the plasma. Thus, even a minor variation in the plasma power will significantly impact the signal intensity during the analyses. Maximum sensitivity in the axial and radial mode

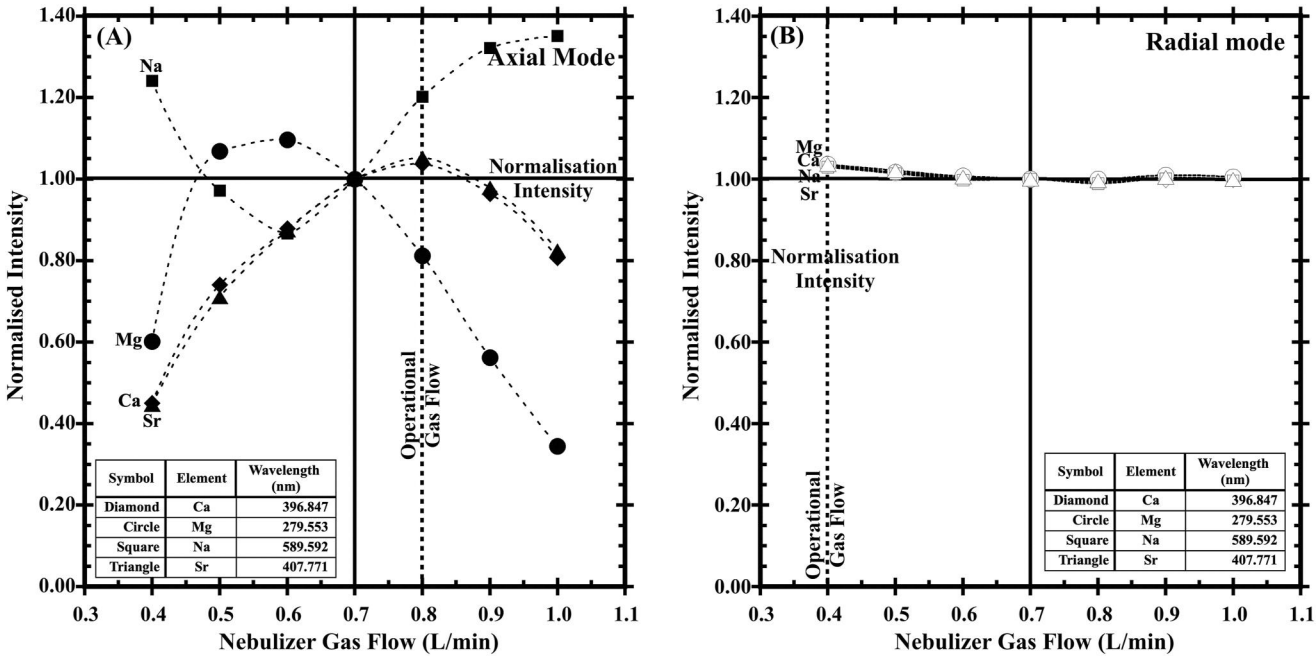

Figure 3. Response of signal intensity for Ca, Mg, Na, and Sr to variable nebulizer gas flow rate (in L/min) under typical operational conditions. The nebulizer gas flow rate is plotted on the *x*-axis with normalized intensity (counts per second) on the *y*-axis. Panel (a) axial mode of acquisition; Panel (b) radial mode of acquisition. The normalized intensities are represented by the following symbols: Ca-diamond, Mg-circle, Na-square, and Sr-triangle. The solid and open symbols represent the analysis performed in axial and radial mode respectively. The axial mode exhibits a greater change in intensity for a unit change (0.1 L/min) in gas flow.

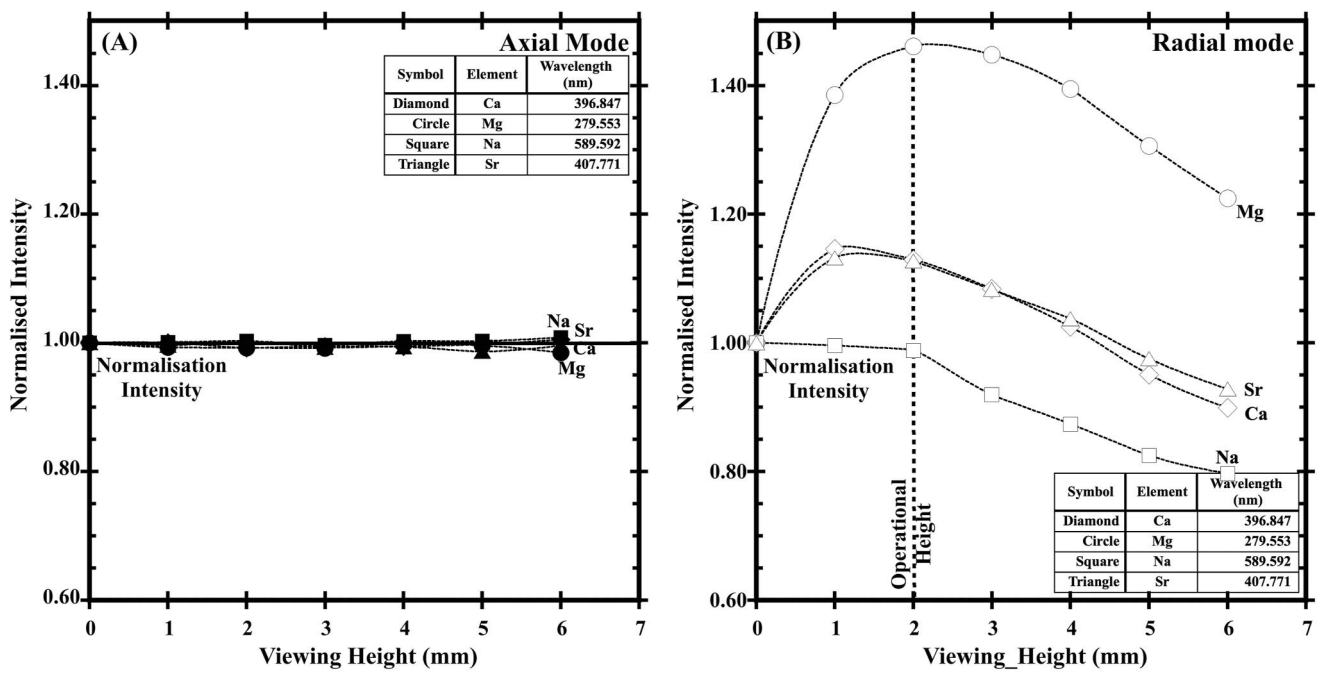

Figure 4. Determination of torch position for optimal signal intensity on Ca, Mg, Na, and Sr under typical operational conditions. Panel (a) axial mode of acquisition; Panel (b) radial mode of acquisition. The viewing height and the normalized intensity (counts per second) are plotted on the *x* and *y*-axis respectively. The results demonstrate that the torch position has minimal to no impact in the axial mode whereas in radial mode the sensitivity shows large-scale variation (−20 to +40%) with viewing height.

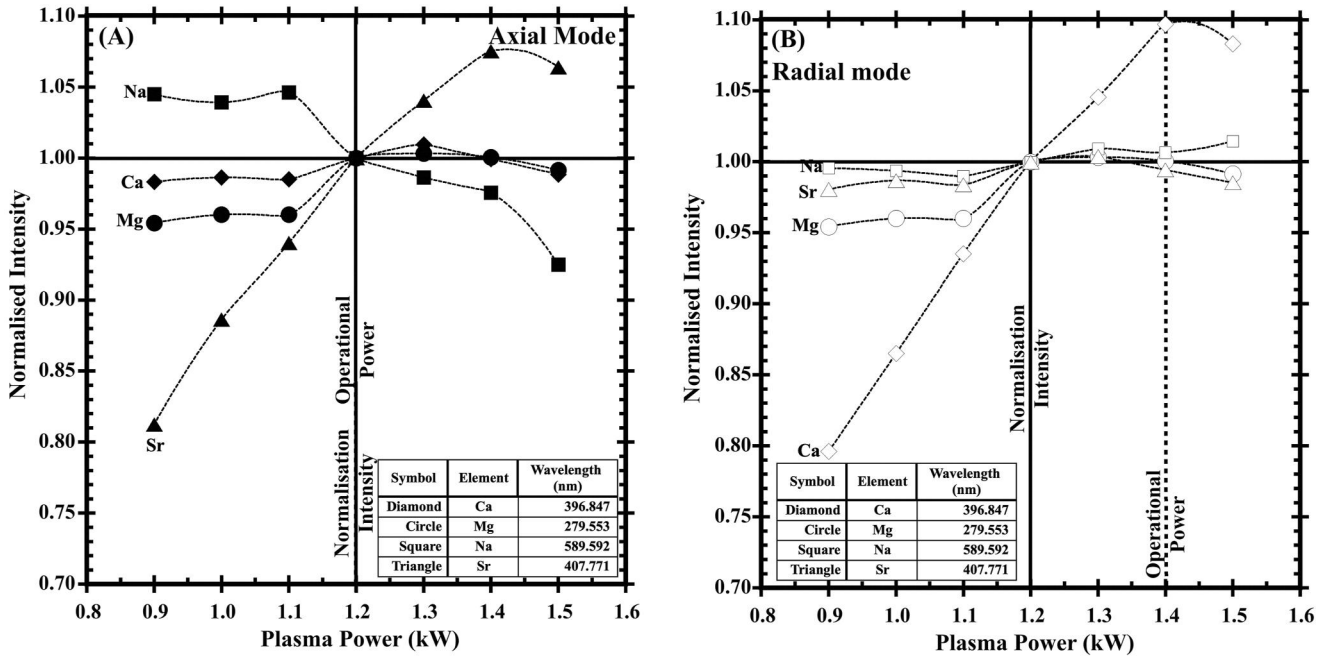

Figure 5. Variation in signal intensity for Ca, Mg, Na, and Sr for different plasma power (kW) under typical operational conditions. Plasma power and normalized intensity (counts per second) are represented on the *x* and *y*-axis respectively. Panel (a) axial mode of acquisition; Panel (b) radial mode of acquisition. The normalized intensities are denoted by the following symbols: Ca-diamond, Mg-circle, Na-square, and Sr-triangle. The solid and open symbols represent the analysis performed in axial and radial mode respectively. The axial mode exhibits a greater change in intensity for a unit change (0.1 L/min) in gas flow.

was observed at 1,200 and 1,400 W respectively (Figure 5). However, the focus was on the axial mode of detection, so we opted for an R.F. power of 1,200 W.

3.1.6. Selection of Elemental Line Sensitivity for Analyses

Marine carbonates contain 40% Ca in the shell and the acid-dissolved samples contain >99% Ca (cation) matrix in solution. Calcium, an alkali earth metal, has a self-matrix effect during ICP-OES based concentration determination. This self-matrix effect is defined as the decrease in excitation temperature and thus the elemental sensitivity with an increase in the concentration of the analyte in the sample (Ramsey et al., 1987). The impact of self-matrix or self-adsorption can be observed in the non-linearity of the elemental sensitivity line at higher concentrations of analyte (de Villiers et al., 2002; Schrag, 1999). The degree of non-linearity or the curvature of the emission lines is more profound in the sensitive spectrum that is, the emission lines with a highest sensitivity demonstrate the largest deviation from linearity at higher analyte concentrations. To maintain linearity of calcium calibration across a large range of concentration, it is critical to optimize the instrumental plasma parameters and to choose the right emission line, based on sensitivity, self-matrix, and self-adsorbent effects, for accurate determination. Following this selection criteria, we selected seven calcium emission lines namely, Ca 315.887 nm, Ca 317.933 nm, Ca 318.127 nm, Ca 373.690 nm, Ca 393.366 nm, Ca 396.847 nm, and Ca 422.673 nm. The calibration curves generated across a concentration range of 0–300 ppm demonstrate (Figure 6) the non-linear behavior or the curvature for specific emission lines of calcium such as Ca 396.847 nm and Ca 393.366 nm. This observation is true even at the range of moderate to high Ca concentrations of 100 ppm. This range is significantly lower than the expected Ca concentration in foraminifera samples. Thus, these lines were not utilized for concentration measurements.

The line with highest elemental sensitivity (Ca 396.847 nm) demonstrates maximum non-linearity with increasing Ca concentration which is in accordance with the self-matrix effect (Figure 6). For example, the signal intensity of calcium emission at 396.847 nm saturates the detector at calcium concentrations of <20 and <100 ppm for axial and radial viewing modes respectively. Thus, this emission line was avoided during sample analysis. However, for mass-limited samples, one may consider utilizing the 396.847 nm Ca emission line because of its high

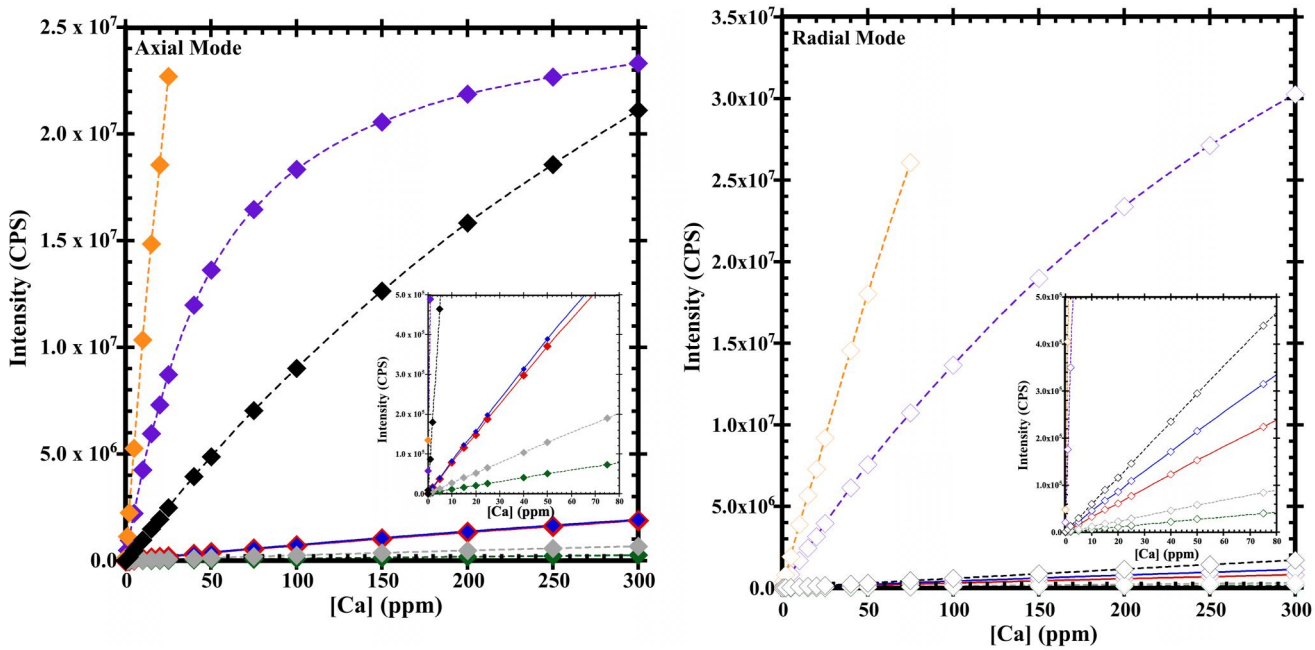

Figure 6. Calcium emission lines specific response of sensitivity for a large range of Ca concentration of 0–300 ppm Ca. The *x*-axis represents Ca concentration, while the *y*-axis represents calcium intensity in counts per second. Wavelengths exhibiting high sensitivity reach saturation at lower Ca concentrations (self-matrix effect) and commonly exhibit curvature/nonlinear response to increasing concentrations. The Ca emissions at: Ca 315.887 nm, Ca 317.993 nm, Ca 318.127 nm, Ca 373.690 nm, Ca 393.366 nm, Ca 396.847 nm, and Ca 422.673 nm, are represented by red, blue, green, gray, violet, orange, black symbols respectively. Solid and open symbols represent the results in axial and radial modes respectively. The accompanying table provides additional information, on the wavelength, R-squared (RSQ) values, and saturation concentration. Panel (a) depicts axial mode detection, while Panel (b) corresponds to radial mode detection. The graph in the inset highlights results in the concentration range from 0 to 80 ppm Ca.

sensitivity and linear behavior. The next sensitive calcium emission line at 393.366 nm is also characterized by curvature at higher calcium concentrations in both the radial and axial viewing modes and was thus ruled out. The calcium emission line at 422.673 nm demonstrated nonlinearity in axial mode at [Ca] ≥50 ppm, however in radial mode no such nonlinearity was observed. The other four calcium emission lines demonstrated linear behavior in both axial and radial modes over a Ca concentration range of 0–300 ppm. Among the four emission lines which fulfilled the selection criteria, we opted for the 315.887 nm line due to its comparatively high sensitivity and linear behavior across a large concentration range. Additionally, the 317.993 Ca intensity line can also be utilized due to its linearity in both axial and radial modes across a wide range of Ca concentrations. In summary, to minimize the self-matrix effect we avoid selecting Ca emission wavelengths of 422.673, 396.847, and 393.366 nm. Based on sensitivity and linearity we opted for 315.887 nm line in both detection modes. Table S1 in Supporting Information S1 presents the values for wavelength and intensity.

The presence of elements like Na, Mg, and Sr can experience signal suppression due to the large abundance of an easily ionizable element (EIE) like Ca in the matrix. In carbonate matrices, whether biogenic or abiogenic, the relative abundance of Na, Mg, and Sr is generally low thus the analysis and determination of these elements must be carried out in the axial mode. As a result, all subsequent experiments described in this paper were performed using the axial mode of detection. The matrix effect of an EIE like Ca was tested on other elemental emission lines for Na, Sr, and Mg with increasing concentration of Ca in the matrix. We conducted additional tests on the selected elemental lines to assess how the presence of a calcium-based matrix affects the sensitivity and linearity of other elements like sodium (Na), magnesium (Mg), and strontium (Sr). To accomplish this, we analyzed standards with progressively increasing concentrations of calcium while maintaining fixed concentrations of Na, Mg, and Sr. The results of the experiment are visualized in Figure 7. Each solution that was analyzed contained a constant concentration of 5 ppm for sodium (Na), magnesium (Mg), and strontium (Sr). However, the calcium (Ca) concentration varied from 0 to 300 ppm. The intensities of sodium, magnesium, and strontium were then normalized to a 5 ppm multi-element solution for comparison. We observe that there is a strong matrix effect arising from calcium on these elements and thus we opt for specific emission lines for Na (589.592), Mg

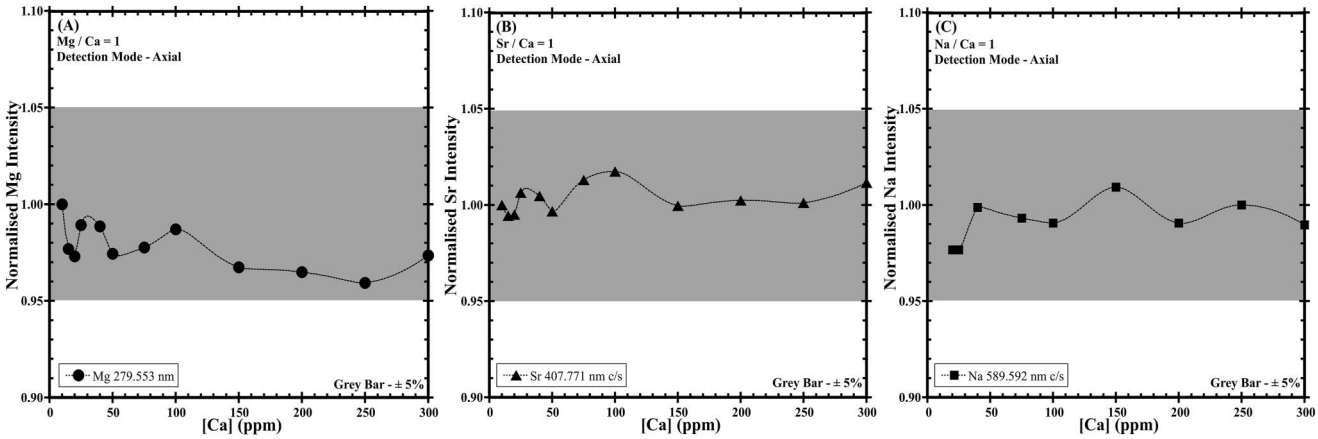

Figure 7. This experiment examines the impact of the self-matrix effect of Ca on Mg, Sr, and Na, by analyzing the intensities of various elemental lines within the concentration range of 5–300 ppm Ca. The solution is prepared in a manner that ensures the same concentration of Mg, Na, and Sr of 5 ppm across the concentration range of 0–300 ppm Ca. Subsequently, the values are normalized using the respective first value as the reference point. It is observed that some elemental lines for Mg, Sr, and Na do not exhibit any self-matrix effect as the Ca concentration increases. The *x*-axis represents the Ca concentration, while the *y*-axis represents the normalized intensity of (a) Mg, (b) Na, and (c) Sr. All the measurements depicted in the figure were conducted in the axial mode.

(279.553), and Sr (407.771) in axial mode which demonstrated minimal to no matrix effect. The results of this experiment are presented in Figure 7. Note that, even in the radial mode, these emission lines show no matrix effect thus for samples with high concentrations of Na, Mg, and Sr one may utilize the radial mode of detection such as the determination of Sr/Ca in coral samples. By utilizing these specific elemental emission lines for analysis, we achieve a high level of accuracy and precision. Through multiple repetitions of the analysis on the same sample, we consistently observe long-term precision better than 1%.

The influence of the matrix effect on the elemental ratio space of (Na/Ca, Mg/Ca, and Sr/Ca) is also examined on the selected elemental lines (Mg 285.533/Ca 315.887, 589.592/Ca 315.887, and Sr 407.771/Ca 315.887 lines.). Calcium carbonate samples are dissolved and analyzed for elemental ratios at different Ca concentrations spanning from 5 to 250 ppm Ca. The findings of this experiment are illustrated in Figure 8, clearly indicating that the elemental ratios remain consistent across the entire range of Ca concentrations, positioning closely with the true average value of the sample.

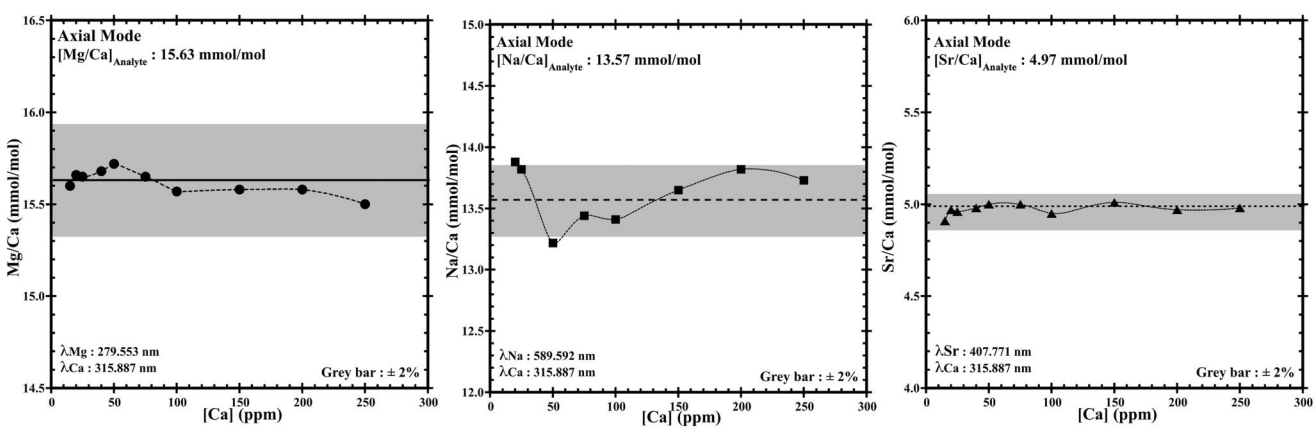

Figure 8. The test investigates the impact of the self-matrix effect on the selected wavelength line of measured Mg/Ca, Na/Ca, and Sr/Ca values in relation to Ca concentration. The same sample is analyzed with varying concentrations of Ca, ranging from 5 to 250 ppm. The Panel (a) representing Mg 285.533/Ca 315.887, (b) representing Na 589.592/Ca 315.887, and (c) representing Sr 407.771/Ca 315.887 lines. It can be observed that the ratio of minor and trace elements to calcium remains constant throughout the concentration range. This indicates that the selected wavelengths do not exhibit any matrix effect caused by increasing calcium concentration. The gray bar in all panels represents a 2% error range from the average value.

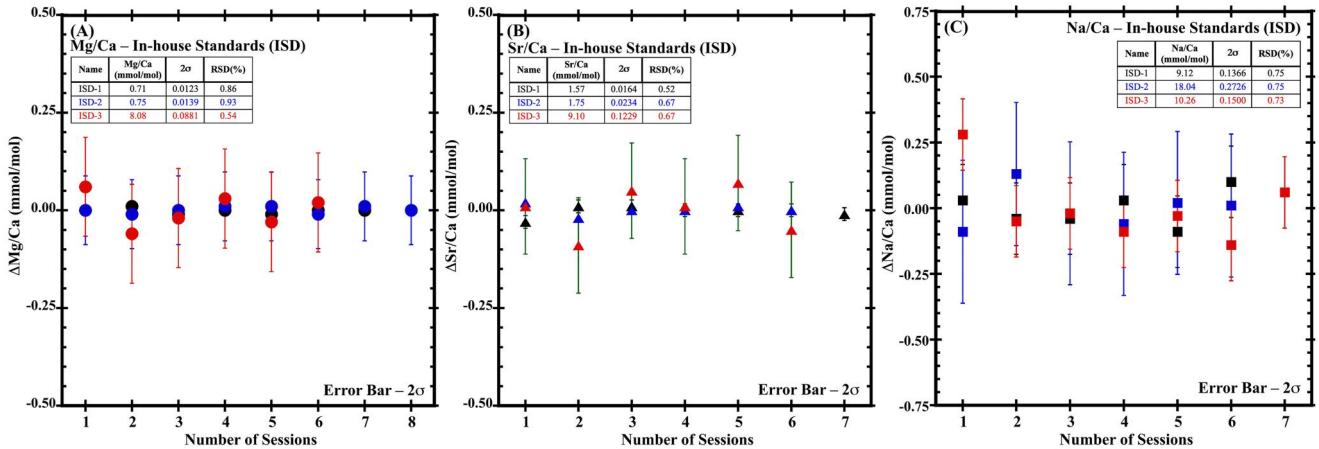

Figure 9. The figure shows the long-term reproducibility of Mg/Ca, Sr/Ca, and Na/Ca for in-house standards. The reproducibility for each element is represented by circles, triangles, and squares, corresponding to Mg/Ca, Sr/Ca, and Na/Ca, respectively. The ISD-1, ISD-2, and ISD-3 standards are differentiated by black, blue, and red colors. The error bars in the graph represent 2σ. The deviations from the average value (on the *y*-axis) are plotted against the session numbers (on *x*-axis). In the figure, you can find the averaged measured value of each standard, along with their 2SD uncertainty and the relative standard deviation (RSD %).

3.2. Long-Term Accuracy and Precision

To summarize, the long-term precision of the ICP-OES method was assessed by repeat analysis of three in-house standards. We acquired a collection of biogenic carbonate samples (corals from 20°S) during the Southern Ocean expedition (2020–2021). These specimens were finely powdered to create a homogenized sample. Aliquots of the homogenized samples underwent chemical cleaning following the protocol outlined in the manuscript. These in-house standards covered a range of Mg/Ca, Sr/Ca, and Na/Ca values as follows: Mg/Ca ranged from 0.71 to 8.08 mmol/mol; Sr/Ca ranged from 1.57 to 9.10 mmol/mol; and Na/Ca values ranged from 9.12 to 18.04 mmol/mol. The long-term reproducibility of the present method was determined through repeat analysis of these in-house standards across 7 to 8 analytical sessions spanning 4 months. In each session, the standards were measured 4–5 s times, and the deviation of the sessional average from the long-term average is plotted in Figure 9. We report a precision of better than 1% for Mg/Ca, Sr/Ca, and Na/Ca determination by the present method.

During each analytical session, the samples were prepared from a primary stock solution at 60 ppm Ca, (Schrag, 1999), using the same acid as the remaining samples. The stability of the stock solutions was confirmed by cross-checking with different sets of standards over a period of 1 year. The long-term accuracy and precision of our method were found to be comparable or even better than other OES methods (Schrag, 1999). For instance, the long-term precision for Mg/Ca, Na/Ca, and Sr/Ca values was less than 1% (Figure 9).

3.3. Analyses on ICP-QQQ-MS

The trace elemental to calcium ratios were determined by Agilent 8900 ICP-QQQ-MS installed at IISc, Bangalore. All the samples and standards were analyzed in a 2% HNO_3 matrix. Analytes were introduced into a c-type self-aspirating concentric nebulizer into a peltier cooled quartz Scott-type spray chamber. The spray chamber was maintained at a constant temperature of 2°C. An integrated quartz torch with 2.0 mm injector was used. An optimal uptake time of 55 s, and stabilization time of 10 s with a washout time of 180 s was determined through time resolved analyses (Figure 10).

3.3.1. Comparison Between Quartz and Teflon Spray Chamber

The utilization of hydrofluoric acid for improved washout of boron is well established (Misra et al., 2014). This requires the use of a relatively expensive Teflon spray chamber for sample introduction. Additionally, the sensitivity of elements is lower in Teflon spray chambers compared to that in quartz (Figure 11). HR (high-resolution) mass spectrometers are characterized by significantly higher sensitivity than ICP-QQQ-MS. Thus, the use of a Teflon spray chamber and HF acid for HR-ICP-MS based B/Ca (and other ME/Ca) doesn't compromise accuracy and precision. In contrast, for quadrupole-based instruments, a higher sensitivity is desirable since it

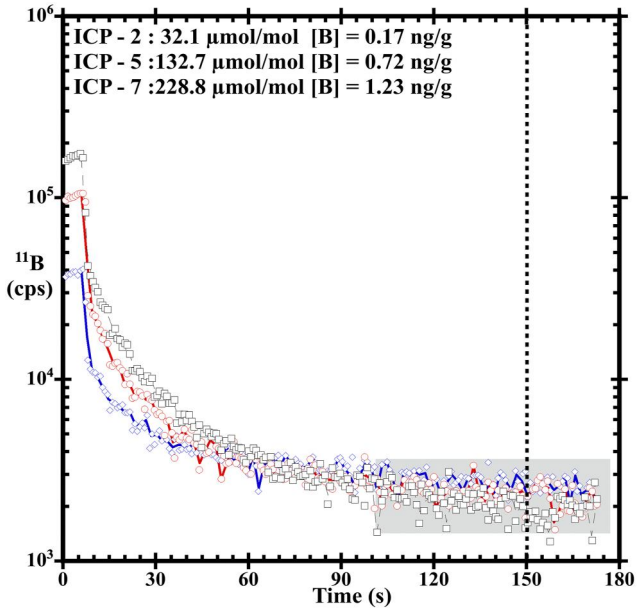

Figure 10. The boron washout time in the quartz spray chamber was determined using three standards with different B/Ca ratios: 32.1 µmol/mol (represented by blue squares), 132.7 µmol/mol (represented by red circles), and 228.8 µmol/mol (represented by black squares). The analyses were performed by alternating between these three standards and an acid blank, all having the same matrix composition. The *Y*-axis of the graph represents the ^{11}B counts plotted on a logarithmic scale, while the *X*-axis represents the time in seconds. The gray bar represents the section of identical blank values obtained prior to the introduction of the B/Ca standard to the spray chamber.

allows for the determination of mass-limited samples. To avoid the usage of corrosive acid like HF and to achieve high sensitivity for boron, we have opted to use a quartz spray chamber which provides a higher signal to noise ratio in a more cost-effective way. However, the use of a quartz spray chamber rules out the possibility of using HF. Thus, to prevent the buildup of boron in the spray chamber leading to a memory effect, we have a prolonged washout time of 180 s. This ensures a quantitative washout of boron from the spray chamber thereby eliminating the carry over effect between samples (Figure 10). Similarly in the non-collision reaction mode, sensitivity is relatively higher for low-mass elements compared to the collision mode. However, the signal-to-noise ratio remains largely similar between the two modes (Figure 12).

3.3.2. Instrument Settings

The instrument was tuned for optimal sensitivity and peak shape across the mass range of ^{7}Li to ^{238}U prior to each analytical session. Elements with isobaric interferences like K, Mn, and Fe were measured in CRC mode. The CRC mode was tuned for minimum blanks on ^{80}Se (^{40}Ar^{40}Ar), ^{39}K (Ar+), and ^{56}Fe (^{40}Ar^{16}O) in 2% HNO_3, and a maximum signal to noise ratio for ^{39}K and ^{56}Fe masses. The tuning of CRC primarily focused on lens parameters and collision cell gas flows. The choice of isotope of a particular element utilized for the determination of elemental concentration was primarily based on its relative abundance and the magnitude of possible plasma/matrix based polyatomic interferences on the different isotopes of the same element.

Elemental Ca ratios were calculated in offline mode. We utilized an external calibration based on a series of multi-element standards at fixed Ca

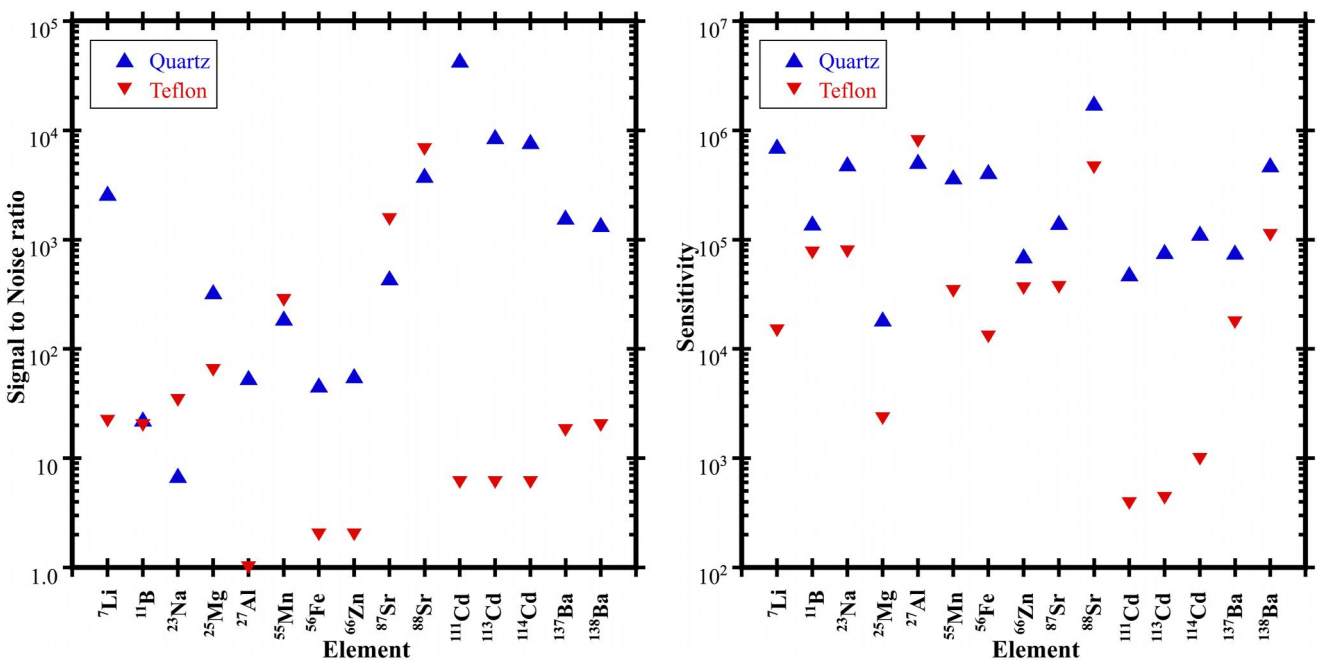

Figure 11. The graph presents a comparison of panel (a) signal-to-noise ratio and panel (b) sensitivity between quartz and Teflon spray chambers. The *y*-axis represents the signal-to-noise ratio in panel (a) and sensitivity in panel (b), while the *x*-axis represents the element names. The data for the Quartz and Teflon spray chamber is represented by blue up pointed and red down pointed triangles. Observations indicate that both the signal-to-noise ratio and sensitivity are higher for the quartz spray chamber compared to the Teflon spray chamber. As a result, for improved resolution and precision, we have chosen to utilize the quartz spray chamber in our study.

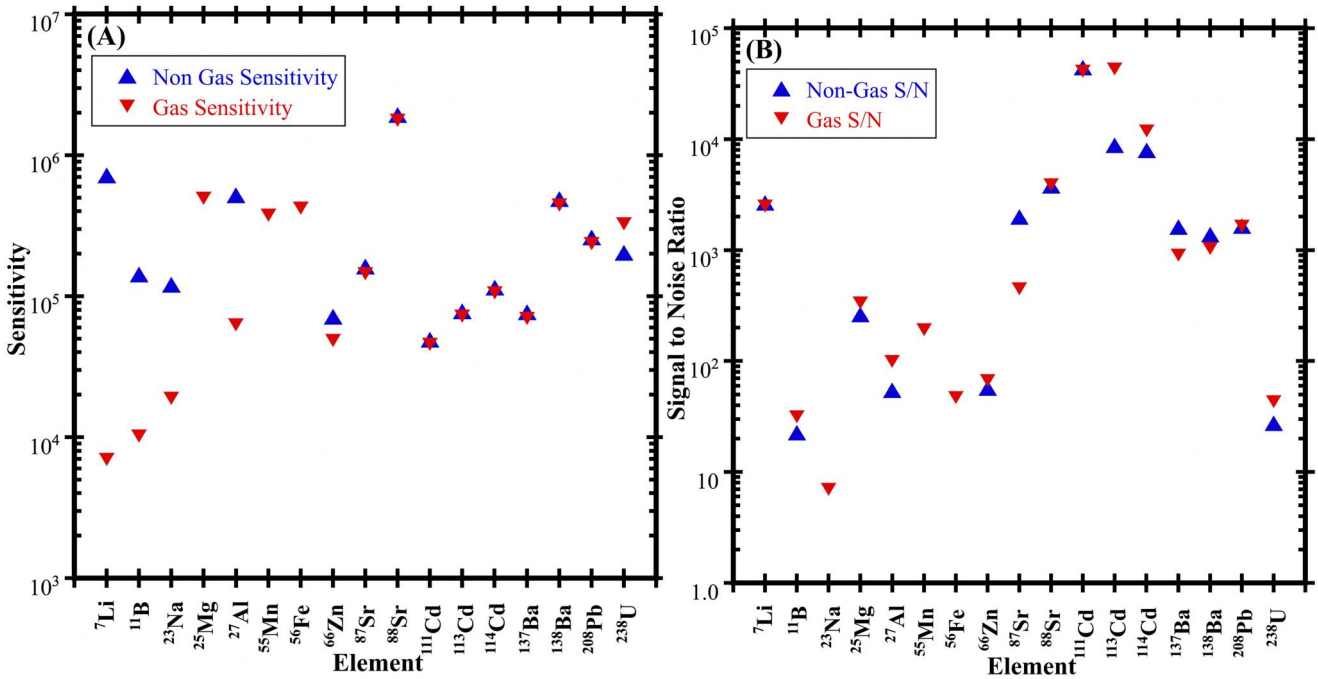

Figure 12. The graph presents a comparison between non-collision mode and collision reaction mode in the quartz spray chamber, specifically focusing on panel (a) signal-to-noise ratio and panel (b) sensitivity. The *y*-axis represents the signal-to-noise ratio in panel (a) and sensitivity in panel (b), while the *x*-axis corresponds to the element names. The data for the non-collision reaction mode and collision mode are represented by blue up-pointed and red down-pointed triangles, respectively. Observations show that in the non-collision reaction mode, sensitivity is relatively higher for low-mass elements compared to the collision mode. However, the signal-to-noise ratio remains largely similar between the two modes.

concentrations (ICP standard Table S2 in Supporting Information S1: the Cambridge set of standards). The raw intensities were blank corrected, converted to ME/Ca ratio space, drift corrected, and then normalized. The normalized ratios are converted to concentration (mmol/mom or μmol/mol) based on the slope of the calibration line (de Villiers et al., 2002). Every analytical session we ensured that the calibration lines have an RSQ ranging from ≥0.99 to ≥0.9999 (The supplementary material includes calibration curves for both ICP-OES and ICP-QQQ-MS analyses. These can be referenced in Figures S1 and S2 in Supporting Information S1).

The instrument was operated with an integration time of 0.1 and 0.2 s for minor (e.g., Na, Mg, Sr) and trace elements (e.g., Cd, Ba, U) respectively. The increased integration time on the elements with low abundance provided better counting statistics. Replicates/Sweeps were set at 9/9 for each analysis as it provides good accuracy and precision with minimal mass consumption. The complete list of elements and the integration time of each isotope is given in Table 3. Based on the selected integration time and the number of Replicates/Sweeps, the total acquisition time for the entire range of masses is about 30 s. The instrumental drift was minimized by preconditioning the cones with 20 ppm Ca for an hour prior to every analytical session.

3.3.3. Limit of Detection

In analytical chemistry, the limit of detection (LOD) refers to the lowest concentration or amount of an analyte that can be reliably detected with a given method. It is a measure of sensitivity and represents the lower limit at which an analyte can be distinguished from background noise or interference. The LOD is an important parameter in analytical methods as it helps determine the sensitivity and performance of the method.

Achieving a low LOD is desirable in many analytical applications, especially in fields such as paleoclimate, environmental monitoring, pharmaceutical analysis, and forensic sciences, where trace-level detection is required. The LOD allows analyses to determine the minimum concentration or amount of an analyte that can be reliably detected and quantified using a specific analytical technique. The LOD is a measure of each element calculated utilizing the formula:

$$\text{LOD} = \left(\frac{3 * \text{Standard deviation of the Standard}}{\text{Analytical Sensitivity of } \frac{\text{ME}}{\text{Ca}}} \right) * \left(\frac{\text{ME}}{\text{Ca}} \right) \text{mol/mol}$$

The LOD in this study is determined by utilizing the ICP-4 standard (Table S2 in Supporting Information S1), which represents the average composition of a foraminifera matrix. The ICP-4 standard is run five times consecutively to obtain multiple measurements. The average value of ME/Ca across all runs is considered as the analytical sensitivity for ME/Ca, and the standard deviation is calculated to assess the variability for a specific element. To determine the LOD, the obtained standard deviation ME/Ca value is multiplied by 3 and then divided by the average analytical sensitivity. Subsequently, the resulting value is multiplied by the standard value of the corresponding ME/Ca of the ICP-4 standard. Table 4 provides the LOD values for ME/Ca pertaining to our instrumental tuning.

3.3.4. Measurement Protocol

Elemental concentrations in both biogenic and abiogenic calcite ranges from low ppt levels (e.g., Cd, U) to high ppb levels (e.g., Mg, Sr) when measuring at a fixed calcium concentration of ≤100 ppm. The accurate and precise determination of elements that are at sub nanogram level in the analyte are limited at both instrumental and procedural blank. Thus, maintaining low laboratory blanks is critical for accurate determination. To minimize elemental blanks, dissolution of chemically cleaned calcite, dilution of samples, and preparation of standards were all done in double distilled nitric acid (diluted to appropriate strength).

All PFA Teflon® vials and beakers used for sample preparation and acid storage were boiled in a reagent grade ∼50% (v/v) HCl followed by ∼50% (v/v) HNO_3 and then rinsed with 18.2 Ω MilliQ-water. Drying of laboratory ware was carried out in a custom-made evaporation cabinet fitted with second-stage boron free PTFE HEPA filtration. For cleaning of LDPE vials and beakers, we utilized a similar strategy with lower normality (∼10%(v/v)) acid. All acids and standards used for chemical cleaning, leaching, dissolution, and analyses of carbonate samples were prepared using double distilled acids with 18.2 Ω MilliQ water. Sub-boiling distillation of acids was performed with a Savillex® DST 4000.

Calcite samples are commonly analyzed at a fixed Ca concentration to ensure an identical matrix effect on both standards and samples. At high Ca concentration (>100 ppm), there is a possibility of calcium deposition on both the sampling and skimmer cones thereby reducing the signal intensity and causing instrumental drift. Thus, to avoid these analytical artifacts, calcite samples are analyzed at a fixed calcium concentration of ≤100 ppm (Misra et al., 2014; Yu et al., 2007).

3.3.5. Concentration Selection and Concentration Mismatch

To determine the appropriate calcium (Ca) concentration for our ME/Ca experiments on the ICP-QQQ-MS, we conducted an experiment involving multiple runs of a particular standard at different concentrations. The aim was to assess the percentage error from the true value and identify a Ca concentration that provides good precision. Running samples at low Ca concentrations presents challenges, as elements like Cd and Ba are present in very low concentrations, potentially at or below the detection limit. Additionally, for samples with limited mass, running at high concentrations is not feasible.

The experiment consisted of running the standard at calcium concentrations of 5, 10, 15, 20, 30, and 50 ppm. The results of this experiment are illustrated in Figure S3 in Supporting Information S1. It was observed that at lower concentrations, the error percentage is higher, but as the concentration increases, the error decreases and stabilizes at around 20 ppm Ca. Based on this experiment, we determined that the optimum concentration for precisely determining the trace element to calcium ratio on the ICP-QQQ-MS is approximately 20 ppm Ca.

Furthermore, we conducted another experiment to evaluate the impact of concentration mismatch on the accuracy and precision of measurements. In this experiment, we measured similar solutions with different Ca concentrations. The results of this experiment are presented in Figure S4 in Supporting Information S1. It is evident that a concentration mismatch between samples and standards leads to a decrease in accuracy. Therefore, to obtain

Table 5
Long-Term Precision and Accuracy on ICP-QQQ-MS

ME/43Ca	Units	(Mode)	Average	2 * STDEV	RSD (%)
$^{7}Li/^{43}Ca$	µmol/mol	Non gas	18.55	0.180	0.48
$^{11}B/^{43}Ca$	µmol/mol	Non gas	149.49	0.529	0.18
$^{23}Na/^{43}Ca$	mmol/mol	Gas	8.42	0.092	0.55
$^{24}Mg/^{43}Ca$	mmol/mol	Gas	4.21	0.025	0.30
$^{25}Mg/^{43}Ca$	mmol/mol	Non gas	4.18	0.057	0.69
$^{25}Mg/^{43}Ca$	mmol/mol	Gas	4.00	0.012	0.15
$^{27}Al/^{43}Ca$	mmol/mol	Non gas	0.21	0.002	0.38
$^{27}Al/^{43}Ca$	mmol/mol	Gas	0.20	0.001	0.20
$^{55}Mn/^{43}Ca$	µmol/mol	Gas	26.69	0.074	0.14
$^{56}Fe/^{43}Ca$	mmol/mol	Gas	0.15	0.044	0.14
$^{66}Zn/^{43}Ca$	µmol/mol	Non gas	16.72	0.055	0.17
$^{66}Zn/^{43}Ca$	µmol/mol	Gas	16.51	0.350	1.06
$^{87}Sr/^{43}Ca$	mmol/mol	Non gas	1.90	0.033	0.87
$^{87}Sr/^{43}Ca$	mmol/mol	Gas	1.76	0.021	0.59
$^{88}Sr/^{43}Ca$	mmol/mol	Gas	1.86	0.010	0.27
$^{111}Cd/^{43}Ca$	µmol/mol	Non gas	0.36	0.029	4.08
$^{113}Cd/^{43}Ca$	µmol/mol	Non gas	0.34	0.005	0.68
$^{114}Cd/^{43}Ca$	µmol/mol	Non gas	0.34	0.004	0.64
$^{137}Ba/^{43}Ca$	µmol/mol	Non gas	11.87	0.125	0.53
$^{138}Ba/^{43}Ca$	µmol/mol	Non gas	11.88	0.034	0.14
$^{238}U/^{43}Ca$	nmol/mol	Non gas	90.61	0.004	0.43

precise and accurate measurements, it is recommended to run the samples and standards at the same concentration. The results indicate a decrease in accuracy by approximately 10% from the true value due to concentration mismatch in certain elements such as Li, Mn, Zn, and Cd.

3.4. Long-Term Accuracy and Precision

The long-term accuracy and precision of the elemental/calcium ratio on OES and ICP-QQQ-MS were determined by repeat measurements of our in-house calcium standards (Table 5). During every analytical session, the samples are prepared from the primary stock solution at 60 ppm Ca for OES and at 20 ppm Ca for ICP-MS using the same acid that we used to prepare the other samples. Cross-checking the standards with the different sets of standards revealed that the stock solutions were stable for at least 1 year. Our method's long-term accuracy and precision are comparable or better than other ICP-MS methods (Table 5). For example, the long-term precision of the Li/ca value is 0.48%, and B/Ca can be analyzed at the precision of 0.18%. The precision of Mg/Ca, Sr/Ca, and Na/Ca are 0.15%, 0.27%, and 0.55% respectively. We achieved a comparable level of precision for the lower ME/Ca ratios, such as Li/Ca (~2.48 µmol/mol, RSD = 0.79%), Mg/Ca (~0.73 mmol/mol, RSD = 0.87%), and Cd/Ca (~0.04 µmol/mol, RSD = 0.60%) (Figure S5 in Supporting Information S1) which is an improvement compared to previously reported precisions (Green et al., 2003; Lea & Martin, 1996; Marchitto et al., 2000; Rosenthal et al., 1999; Russell et al., 1994; Schrag, 1999; Wara et al., 2003; Yu et al., 2005). The Al/Ca and Fe/Ca ratios are used to assess the quality of foraminiferal samples. High levels of Al/Ca and Fe/Ca can indicate contamination, while low levels can suggest that the samples have been effectively cleaned.

3.5. Comparison of ICP-OES and ICP-QQQ-MS Methods and Data

We selected 4–5 individual *G. bulloides* specimens from the 300–355 µm size range. Under a microscope, the samples were cracked open and treated for clay removal. Subsequently, oxidative cleaning was performed using

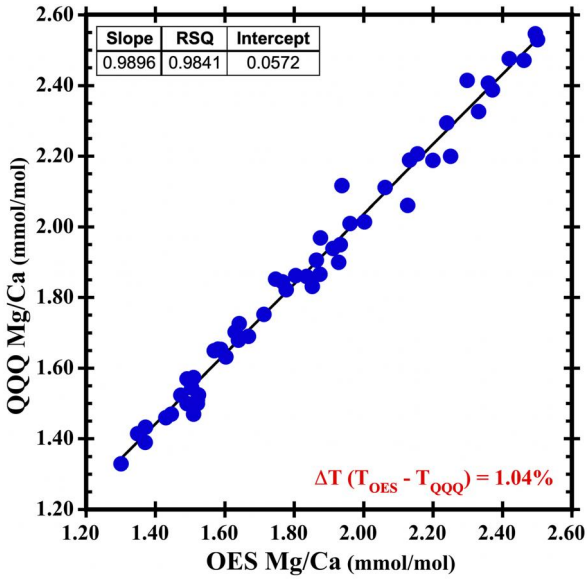

Figure 13. The graph shows the Mg/Ca ratios obtained from ICP-OES and ICP-QQQ-MS analysis of *G. bulloides* samples retrieved during the Southern Ocean Expedition—11. The *x*-axis shows the Mg/Ca (mmol/mol) ratio from ICP-OES, and the *y*-axis shows the Mg/Ca (mmol/mol) ratio from ICP-QQQ-MS. The correlation between the ICP-QQQ-MS and ICP-OES measurements is approximately 99%. The average temperature difference calculated using Mg/Ca of both instruments is 1.04%. The graph shows a strong correlation between the two measurement methods.

1% H_2O_2 in 0.1 N NaOH, as described by Chanakya and Misra (2022). The samples were then leached with 0.001 N HNO_3 and analyzed for Mg/Ca using both ICP-OES at 60 ppm Ca and ICP-QQQ-MS at 20 ppm Ca. The cross plot (Figure 13) of the OES and QQQ data demonstrates a strong correlation, indicating the accuracy and precision of our method. This further exemplifies the strength and reliability of the method outlined in this paper.

4. Conclusions

We have developed a three step analysis strategy for precise (≤1%, 1σ) determination of trace element to calcium ratios from low mass (<40 μg) carbonate samples. Our analysis strategy involves: (a) determination of calcium concentration in the dissolved sample by ICP-OES; (b) determination of major element to calcium ratio (Na/Ca, Mg/Ca, and Sr/Ca) by ICP-OES; and (c) analysis of trace element to calcium ratio using collision cell equipped ICP-QQQ-MS.

High levels of accuracy and precision for metal to calcium determination were achieved by minimizing the instrumental drift and possible matrix effects by conditioning the cones with Ca prior to every analytical session and by analyzing the samples and standards at identical Ca concentration. This rapid analysis method allows us to determine multiple element(s) to calcium ratio from mass-limited $CaCO_3$ samples. A key advantage of the present method is that all analyses (including B/Ca) were performed in a 2% HNO_3 matrix, avoiding any use of HF for fast washout of B. Potential applications of this method include trace element analysis of mass-limited abiogenic and biogenic $CaCO_3$.

Data Availability Statement

The data provided in this paper represent experimental data conforming to established standards. We have provided the data availability at Mendeley Data archive at Ilindra (2023) with license CC BY 4.0, access conditions.

Acknowledgments

We thank the Department of Science and Technology (DST) for funding through the Swarnajayanti Fellowship awarded to SM (SB/SJF/2020–21/10). The Water Technology Institute of DST funded the instrument facility at the Indian Institute of Science (IISc) through the grant Fast Forward to SDG6 (DST/TM/EWO/WTI/2K19/UWS/03 G3).

References

Allen, K. A., Hönisch, B., Eggins, S. M., Haynes, L. L., Rosenthal, Y., & Yu, J. (2016). Trace element proxies for surface ocean conditions: A synthesis of culture calibrations with planktic foraminifera. *Geochimica et Cosmochimica Acta*, *193*, 197–221. https://doi.org/10.1016/j.gca.2016.08.015

Allen, K. A., Hönisch, B., Eggins, S. M., & Rosenthal, Y. (2012). Environmental controls on B/Ca in calcite tests of the tropical planktic foraminifer species Globigerinoides ruber and Globigerinoides sacculifer. *Earth and Planetary Science Letters*, *351–352*, 270–280. https://doi.org/10.1016/j.epsl.2012.07.004

Barker, S., Greaves, M., & Elderfield, H. (2003). A study of cleaning procedures used for foraminiferal Mg/Ca paleothermometry. *Geochemistry, Geophysics, Geosystems*, *4*(9), 8407. https://doi.org/10.1029/2003GC000559

Bentov, S., & Erez, J. (2006). Impact of biomineralization processes on the Mg content of foraminiferal shells: A biological perspective. *Geochemistry, Geophysics, Geosystems*, *7*(1), Q01P08. https://doi.org/10.1029/2005GC001015

Billups, K., Rickaby, R. E. M., & Schrag, D. P. (2004). Cenozoic pelagic Sr/Ca records: Exploring a link to paleoproductivity. *Paleoceanography*, *19*(3), PA3005. https://doi.org/10.1029/2004PA001011

Boyle, E. A. (1981). Cadmium, zinc, copper, and barium in foraminifera tests. *Earth and Planetary Science Letters*, *53*(1), 11–35. https://doi.org/10.1016/0012-821X(81)90022-4

Boyle, E. A. (1988). The role of vertical chemical fractionation in controlling late Quaternary atmospheric carbon dioxide. *Journal of Geophysical Research*, *93*(C12), 15701–15714. https://doi.org/10.1029/JC093iC12p15701

Boyle, E. A., & Keigwin, L. D. (1985). Comparison of Atlantic and Pacific paleochemical records for the last 215,000 years: Changes in deep ocean circulation and chemical inventories. *Earth and Planetary Science Letters*, *76*(1–2), 135–150. https://doi.org/10.1016/0012-821X(85)90154-2

Broecker, W. S., & Clark, E. (2004). Shell weights from the South Atlantic. *Geochemistry, Geophysics, Geosystems*, *5*(3), Q03003. https://doi.org/10.1029/2003GC000625

Carroll, M. L., Johnson, B. J., Henkes, G. A., McMahon, K. W., Voronkov, A., Ambrose, W. G., & Denisenko, S. G. (2009). Bivalves as indicators of environmental variation and potential anthropogenic impacts in the southern Barents Sea. *Marine Pollution Bulletin*, *59*(4–7), 193–206. https://doi.org/10.1016/j.marpolbul.2009.02.022

Chanakya, I. V. S., & Misra, S. (2022). Accurate and precise determination of the boron isotope ratio by QQQ-ICP-MS: Application to natural waters and carbonates. *Journal of Analytical Atomic Spectrometry*, *37*(6), 1327–1339. https://doi.org/10.1039/D2JA00051B

Delaney, M. L. (1989). Uptake of cadmium into calcite shells by planktonic foraminifera. *Chemical Geology*, *78*(2), 159–165. https://doi.org/10.1016/0009-2541(89)90114-9

Delaney, M. L., Bé, A. W., & Boyle, E. A. (1985). Li, Sr, Mg, and Na in foraminiferal calcite shells from laboratory culture, sediment traps, and sediment cores. *Geochimica et Cosmochimica Acta*, *49*(6), 1327–1341. https://doi.org/10.1016/0016-7037(85)90284-4

de Villiers, S., Greaves, M., & Elderfield, H. (2002). An intensity ratio calibration method for the accurate determination of Mg/Ca and Sr/Ca of marine carbonates by ICP-AES. *Geochemistry, Geophysics, Geosystems*, *3*(1), 740. https://doi.org/10.1029/2001gc000169

Elderfield, H., & Ganssen, G. (2000). Past temperature and $\delta^{18}O$ of surface ocean waters inferred from foraminiferal Mg/Ca ratios. *Nature*, *405*(6785), 442–445. https://doi.org/10.1038/35013033

Elderfield, H., Vautravers, M., & Cooper, M. (2002). The relationship between shell size and Mg/Ca, Sr/Ca, $\delta^{18}O$, and $\delta^{13}C$ of species of planktonic foraminifera. *Geochemistry, Geophysics, Geosystems*, *3*(8), 1–13. https://doi.org/10.1029/2001GC000194

Foster, L. C., Finch, A. A., Allison, N., Andersson, C., & Clarke, L. J. (2008). Mg in aragonitic bivalve shells: Seasonal variations and mode of incorporation in Arctica islandica. *Chemical Geology*, *254*(1–2), 113–119. https://doi.org/10.1016/j.chemgeo.2008.06.007

Green, D. R. H., Cooper, M. J., German, C. R., & Wilson, P. A. (2003). Optimization of an inductively coupled plasma-optical emission spectrometry method for the rapid determination of high-precision Mg/Ca and Sr/Ca in foraminiferal calcite. *Geochemistry, Geophysics, Geosystems*, *4*(6), 8404. https://doi.org/10.1029/2002GC000488

Hall, J. M., & Chan, L.-H. (2004). Li/Ca in multiple species of benthic and planktonic foraminifera: Thermocline, latitudinal, and glacial-interglacial variation. *Geochimica et Cosmochimica Acta*, *68*(3), 529–545. https://doi.org/10.1016/S0016-7037(03)00451-4

Ilindra, S. C. (2023). Data for determination of trace elemental composition of $CaCO_3$: Application to mass limited abiogenic and biogenic carbonates [Dataset]. Mendeley Data, V1. https://doi.org/10.17632/w2m5z28cck.1

Kısakürek, B., Eisenhauer, A., Böhm, F., Garbe-Schönberg, D., & Erez, J. (2008). Controls on shell Mg/Ca and Sr/Ca in cultured planktonic foraminiferan, Globigerinoides ruber (white). *Earth and Planetary Science Letters*, *273*(3–4), 260–269. https://doi.org/10.1016/j.epsl.2008.06.026

Lea, D. W., & Martin, P. A. (1996). A rapid mass spectrometric method for the simultaneous analysis of barium, cadmium, and strontium in foraminifera shells. *Geochimica et Cosmochimica Acta*, *60*(16), 3143–3149. https://doi.org/10.1016/0016-7037(96)00184-6

Lea, D. W., Mashiotta, T. A., & Spero, H. J. (1999). Controls on magnesium and strontium uptake in planktonic foraminifera determined by live culturing. *Geochimica et Cosmochimica Acta*, *63*(16), 2369–2379. https://doi.org/10.1016/S0016-7037(99)00197-0

Lear, C. H., Rosenthal, Y., & Slowey, N. (2002). Benthic foraminiferal Mg/Ca-paleothermometry: A revised core-top calibration. *Geochimica et Cosmochimica Acta*, *66*(19), 3375–3387. https://doi.org/10.1016/S0016-7037(02)00941-9

Marchitto, T. M., Curry, W. B., & Oppo, D. W. (2000). Zinc concentrations in benthic foraminifera reflect seawater chemistry. *Paleoceanography*, *15*(3), 299–306. https://doi.org/10.1029/1999PA000420

Marr, J. P., Carter, L., Bostock, H. C., Bolton, A., & Smith, E. (2013). Southwest Pacific Ocean response to a warming world: Using Mg/Ca, Zn/Ca, and Mn/Ca in foraminifera to track surface ocean water masses during the last deglaciation. *Paleoceanography*, *28*(2), 347–362. https://doi.org/10.1002/palo.20032

Marriott, C. S., Henderson, G. M., Crompton, R., Staubwasser, M., & Shaw, S. (2004). Effect of mineralogy, salinity, and temperature on Li/Ca and Li isotope composition of calcium carbonate. *Chemical Geology*, *212*(1–2), 5–15. https://doi.org/10.1016/j.chemgeo.2004.08.002

Martin, P. A., Lea, D. W., Mashiotta, T. A., Papenfuss, T., & Sarnthein, M. (2000). Variation of foraminiferal Sr/Ca over Quaternary glacial-interglacial cycles: Evidence for changes in mean ocean Sr/Ca? *Geochemistry, Geophysics, Geosystems*, *1*(12), 1004. https://doi.org/10.1029/1999GC000006

Misra, S., Owen, R., Kerr, J., Greaves, M., & Elderfield, H. (2014). Determination of δ11B by HR-ICP-MS from mass limited samples: Application to natural carbonates and water samples. *Geochimica et Cosmochimica Acta*, *140*, 531–552. https://doi.org/10.1016/j.gca.2014.05.047

Nehrke, G., Keul, N., Langer, G., de Nooijer, L. J., Bijma, J., & Meibom, A. (2013). A new model for biomineralization and trace-element signatures of Foraminifera tests. *Biogeosciences*, *10*(10), 6759–6767. https://doi.org/10.5194/bg-10-6759-2013

Ramsey, M. H., Thompson, M., & Walton, S. J. (1987). Self-matrix effects as a cause of calibration curvature in inductively coupled plasma atomic emission spectrometry. *Journal of Analytical Atomic Spectrometry*, *2*(1), 33. https://doi.org/10.1039/ja9870200033

Rosenthal, Y., Boyle, E. A., & Slowey, N. (1997). Temperature control on the incorporation of magnesium, strontium, fluorine, and cadmium into benthic foraminiferal shells from Little Bahama Bank: Prospects for thermocline paleoceanography. *Geochimica et Cosmochimica Acta*, *61*(17), 3633–3643. https://doi.org/10.1016/S0016-7037(97)00181-6

Rosenthal, Y., Field, M. P., & Sherrell, R. M. (1999). Precise determination of element/calcium ratios in calcareous samples using sector field inductively coupled plasma mass spectrometry. *Analytical Chemistry*, *71*(15), 3248–3253. https://doi.org/10.1021/ac981410x

Russell, A. D., Emerson, S., Nelson, B. K., Erez, J., & Lea, D. W. (1994). Uranium in foraminiferal calcite as a recorder of seawater uranium concentrations. *Geochimica et Cosmochimica Acta*, *58*(2), 671–681. https://doi.org/10.1016/0016-7037(94)90497-9

Russell, A. D., Hönisch, B., Spero, H. J., & Lea, D. W. (2004). Effects of seawater carbonate ion concentration and temperature on shell U, Mg, and Sr in cultured planktonic foraminifera. *Geochimica et Cosmochimica Acta*, *68*(21), 4347–4361. https://doi.org/10.1016/j.gca.2004.03.013

Schrag, D. P. (1999). Rapid analysis of high-precision Sr/Ca ratios in corals and other marine carbonates. *Paleoceanography*, *14*(2), 97–102. https://doi.org/10.1029/1998PA900025

Smith, C. W., Fehrenbacher, J. S., & Goldstein, S. T. (2020). Incorporation of heavy metals in experimentally grown foraminifera from Sapelo Island, Georgia and Little Duck Key, Florida, U.S.A. *Marine Micropaleontology*, *156*, 101854. https://doi.org/10.1016/j.marmicro.2020.101854

Steinhardt, J., Butler, P. G., Carroll, M. L., & Hartley, J. (2016). The application of long-lived bivalve sclerochronology in environmental baseline monitoring. *Frontiers in Marine Science*, *3*, 1–26. https://doi.org/10.3389/fmars.2016.00176

Stoll, H. M., Schrag, D. P., & Clemens, S. C. (1999). Are seawater Sr/Ca variations preserved in quaternary foraminifera? *Geochimica et Cosmochimica Acta*, *63*(21), 3535–3547. https://doi.org/10.1016/S0016-7037(99)00129-5

Toyofuku, T., Kitazato, H., Kawahata, H., Tsuchiya, M., & Nohara, M. (2000). Evaluation of Mg/Ca thermometry in foraminifera: Comparison of experimental results and measurements in nature. *Paleoceanography*, *15*(4), 456–464. https://doi.org/10.1029/1999PA000460

Wara, M. W., Delaney, M. L., Bullen, T. D., & Ravelo, A. C. (2003). Possible roles of pH, temperature, and partial dissolution in determining boron concentration and isotopic composition in planktonic foraminifera. *Paleoceanography*, *18*(4), 1100. https://doi.org/10.1029/2002PA000797

Wit, J. C., de Nooijer, L. J., Wolthers, M., & Reichart, G. J. (2013). A novel salinity proxy based on Na incorporation into foraminiferal calcite. *Biogeosciences*, *10*(10), 6375–6387. https://doi.org/10.5194/bg-10-6375-2013

Yu, J., Day, J., Greaves, M., & Elderfield, H. (2005). Determination of multiple element/calcium ratios in foraminiferal calcite by quadrupole ICP-MS. *Geochemistry, Geophysics, Geosystems*, *6*(8), 1015. https://doi.org/10.1029/2005GC000964

Yu, J., Elderfield, H., & Hönisch, B. (2007). B/Ca in planktonic foraminifera as a proxy for surface seawater pH. *Paleoceanography*, *22*(2), PA2202. https://doi.org/10.1029/2006PA001347

Yu, J., Thornalley, D. J., Rae, J. W., & McCave, N. I. (2013). Calibration and application of B/Ca, Cd/Ca, and $\delta^{11}B$ in Neogloboquadrina pachyderma (sinistral) to constrain CO_2 uptake in the subpolar North Atlantic during the last deglaciation. *Paleoceanography*, *28*(2), 237–252. https://doi.org/10.1002/palo.20024